

Performance of a PEM fuel cell with oscillating air flow velocity: A modeling study based on cell impedance

Andrei Kulikovsky^{1, a)}

Forschungszentrum Jülich GmbH

Institute of Energy and Climate Research,

IEK-14: Electrochemical Process Engineering

D-52425 Jülich, Germany ^{b)}

A model of PEM fuel cell impedance is developed taking into account imposed harmonic perturbation of the air flow velocity in the cathode channel. The flow velocity modulation with the amplitude proportional to AC amplitude of the cell potential lowers the resistivity R_h due to oxygen transport in channel. When relative amplitudes of velocity and potential oscillations are equal, a complete compensation of R_h occurs. This effect explains experimental findings of Kim et al. (doi:10.1016/j.jpowsour.2008.06.069) and Hwang et al. (doi:10.1016/j.ijhydene.2010.01.064), who demonstrated significant improvement of PEM fuel cell performance under oscillating air flow velocity.

I. INTRODUCTION

PEM fuel cell needs air (oxygen) for protons and electrons conversion into water. Air is usually supplied to the cell cathode through a system of channels. As any other transport process in the cell, oxygen transport through the channel is equivalent to electric resistivity R_h leading to potential loss. In more general terms, one has to speak about impedance Z_h of oxygen transport in the channel^{1,2}.

In 2007, Schneider et al.^{1,2} have attracted attention of fuel cell community to “channel” impedance, a “forgotten player” in the theory of PEMFC impedance. Since that time, a number of experimental^{3–5} and modeling^{6–12} studies of this impedance have been published. At typical air (oxygen) flow stoichiometry of about 2, the contribution of R_h to the total cell resistivity is about 15%¹⁰. Clearly, lowering of R_h would lead to significant improvement of the cell performance.

Kim et al.¹³ and later Hwang et al.¹⁴ experimentally demonstrated dramatic improvement of PEMFC performance under oscillating air flow velocity in the channel. The effect of flow pulsation on the cell performance was more pronounced at lower air flow rates, and the cell performance increased with the amplitude of velocity pulsation¹³. The gain in performance has been attributed to improvement of oxygen transport through the cell due to flow pulsation^{13,14}.

Below, a model for PEMFC impedance operated under oscillating air flow velocity is developed. We show that flow velocity oscillations lead to lowering of oxygen transport impedance in the cathode channel. Under certain relation between velocity and potential oscillation amplitudes, the resistivity of oxygen transport in the channel vanishes. This result supports the general conclusion of Kim et al.¹³ and Hwang et al.¹⁴ that flow pulsation improves oxygen transport in the cell; in this work, we demonstrate the mechanism of this improvement. Further, the model gives a relation between the amplitudes of velocity and potential oscillations, at which the oxygen transport loss in the channel vanishes.

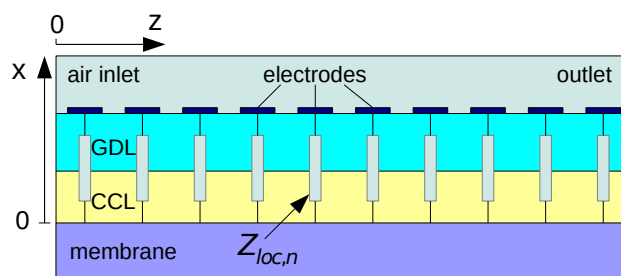


FIG. 1. Schematic of the segmented single-channel cell.

II. MODEL

The model of PEMFC impedance below is extension of the model¹⁵. Consider a segmented PEM fuel cell equipped with the single straight cathode channel (Figure 1). In the channel, oxygen is assumed to be transported along the z -axis, while in the porous layers it is transported in the through-plane direction to the cathode catalyst layer (CCL), where the oxygen reduction reaction (ORR) takes place. The characteristic frequency of oxygen transport in cathode channel is¹⁵

$$f_h \simeq \frac{3.3v}{2\pi L} \quad (1)$$

where v is the air flow velocity and L is the channel length. For typical flow velocity on the order of 10^2 cm s^{-1} and the channel length $L \simeq 100 \text{ cm}$, we get $f_h \simeq 0.5 \text{ Hz}$. This frequency is well below characteristic frequencies for the oxygen and proton transport in porous layers¹⁵, and hence in the analysis of low-frequency phenomena the latter processes can be ignored. The impedance model can thus be derived from the performance model, which takes into account oxygen transport in the channel and faradaic process in the cell.

^{a)}ECS Active member; Electronic mail: A.Kulikovsky@fz-juelich.de

^{b)}Also at:Lomonosov Moscow State University, Research Computing Center, 119991 Moscow, Russia

A. Performance model

Assuming fast proton and oxygen transport in the trough–plane direction, the cell performance is described by the oxygen mass transport equation in the channel

$$\frac{\partial c(t, z)}{\partial t} + v(t) \frac{\partial c(t, z)}{\partial z} = -\frac{j(z)}{4Fh}, \quad c(0) = c_{ref} \quad (2)$$

and proton current conservation equation

$$C_{dl} l_t \frac{\partial \eta(t)}{\partial t} - j(z) = -l_t i_* \left(\frac{c(t, z)}{c_{ref}} \right) \exp \left(\frac{\eta(t)}{b} \right) \quad (3)$$

Here, $c(t, z)$ is the oxygen concentration in the channel, c_{ref} is the reference concentration, z is the distance along the channel, j is the cell current density, h is the channel depth, $\eta(t, z)$ is the ORR overpotential, positive by convention, l_t is the CCL thickness, i_* is the ORR exchange current density, b is the ORR Tafel slope.

Eq.(2) expresses oxygen mass balance assuming plug flow conditions in the channel. The right side of this equation is the stoichiometric flow of oxygen through the membrane–electrode assembly, which agrees with the assumption of fast O_2 transport through the MEA.

Eq.(3) is the proton charge conservation equation in the CCL, assuming that the rate of proton transport through the CCL is fast. This assumption means that the ORR overpotential η is nearly constant through the CCL depth. The overpotential η is also assumed to be independent of the distance z ; this assumption holds if electron conductivity of the cell is large and ohmic losses in the cell are small¹⁶. The first term on the left side of Eq.(3) describes the displacement current during charging/discharging of a double layer, and the term on the right side is the local proton current consumed in the ORR.

In this work, the flow velocity v in Eq.(2) is considered as the time–dependent variable. With the dimensionless variables

$$\begin{aligned} \tilde{t} &= \frac{t}{t_*}, & \tilde{z} &= \frac{z}{L}, & \tilde{j} &= \frac{j}{i_* l_t}, & \tilde{c} &= \frac{c}{c_{ref}}, \\ \tilde{\eta} &= \frac{\eta}{b}, & \tilde{v} &= \frac{v}{v_*}, & \tilde{Z} &= \frac{Z i_* l_t}{b}, & \tilde{\omega} &= \omega t_* \end{aligned} \quad (4)$$

Eqs.(2) and (3) take the form

$$\psi^2 \frac{\partial \tilde{c}}{\partial \tilde{t}} + \tilde{v} \lambda \tilde{J} \frac{\partial \tilde{c}}{\partial \tilde{z}} = -\tilde{j}, \quad \tilde{c}(0) = 1 \quad (5)$$

$$\frac{\partial \tilde{\eta}}{\partial \tilde{t}} - \tilde{j} = -\tilde{c} \exp \tilde{\eta} \quad (6)$$

where ψ is the dimensionless parameter

$$\psi = \sqrt{\frac{4Fhc_{ref}}{C_{dl} b l_t}}, \quad (7)$$

t_* is the characteristic time of the double layer charging

$$t_* = \frac{C_{dl} b}{i_*}, \quad (8)$$

v_* is the time–average flow velocity (see below), λ is the

stoichiometry of air flow corresponding to steady–state flow with the velocity v_*

$$\lambda = \frac{4Fv_* h c_{ref}}{LJ} \quad (9)$$

and \tilde{J} is the mean current density in the cell

$$\tilde{J} = \int_0^1 \tilde{j} d\tilde{z}. \quad (10)$$

A key difference of the system (5), (6) from the system considered in¹⁵ is that \tilde{v} in Eq.(5) is a function of time.

B. Impedance

Now we apply small–amplitude harmonic perturbations to Eqs.(5), (6). The perturbations are of the form

$$\begin{aligned} \tilde{\eta} &= \tilde{\eta}^0 + \tilde{\eta}^1 \exp(i\tilde{\omega}\tilde{t}) \\ \tilde{j} &= \tilde{j}^0 + \tilde{j}^1 \exp(i\tilde{\omega}\tilde{t}) \\ \tilde{c} &= \tilde{c}^0 + \tilde{c}^1 \exp(i\tilde{\omega}\tilde{t}) \end{aligned} \quad (11)$$

Assuming that the inlet flow velocity is modulated with the amplitude proportional to the amplitude of potential perturbation, the time dependence of \tilde{v} can be written as

$$\tilde{v} = 1 + k_v \tilde{\eta}^1 \exp(i\tilde{\omega}\tilde{t}) \quad (12)$$

where $0 \leq k_v \leq 1$ is the real and non–negative modulation amplitude parameter. The unperturbed flow velocity is v_* and hence the static term in Eq.(12) is unity. Note that in experiments of Hwang et al.¹⁴, the mean flow velocity was zero. In this case, the static term in Eq.(12) is zero and the flow velocity has to be scaled using speed of sound, for example. Note also that real k_v means that there is no phase shift between $\tilde{\eta}$ and \tilde{v} oscillations; these oscillations may differ only in amplitude.

Substituting Eqs.(11) and (12) into Eqs.(5), (6) and neglecting terms with the perturbation products, we get equations for the perturbation amplitudes

$$\begin{aligned} \lambda \tilde{J} \frac{\partial \tilde{c}^1}{\partial \tilde{z}} &= - \left(e^{\tilde{\eta}^0} + i\tilde{\omega}\psi^2 \right) \tilde{c}^1 \\ &- \left(e^{\tilde{\eta}^0} \tilde{c}^0 + i\tilde{\omega} \right) \tilde{\eta}^1 - \lambda \tilde{J} \frac{\partial \tilde{c}^0}{\partial \tilde{z}} k_v \tilde{\eta}^1, \quad \tilde{c}^1(0) = 0 \end{aligned} \quad (13)$$

$$\tilde{j}^1 = e^{\tilde{\eta}^0} (\tilde{c}^1 + \tilde{c}^0 \tilde{\eta}^1) + i\tilde{\omega} \tilde{\eta}^1 \quad (14)$$

where Eq.(13) is obtained using Eq.(14). The boundary condition to Eq.(13) means that the inlet oxygen concentration is not perturbed; perturbed is the flow velocity only. Generally, if the flow velocity is perturbed using pressure modulation, the inlet oxygen concentration would also oscillate and the boundary condition to Eq.(13) would read $\tilde{c}^1(0) = \tilde{c}_0^1$. This condition, however, complicates the analysis not changing the main results.

The goal of this work is to demonstrate the effect of inlet velocity modulation on the cell impedance and for the

shapes of static current and oxygen concentration along the channel we take the zero-order solutions¹⁶:

$$\tilde{j}^0 = -\tilde{J}\lambda \ln\left(1 - \frac{1}{\lambda}\right) \left(1 - \frac{1}{\lambda}\right)^{\tilde{z}} \quad (15)$$

$$\tilde{c}^0 = \left(1 - \frac{1}{\lambda}\right)^{\tilde{z}} \quad (16)$$

Eqs.(15), (16) are valid if the cell ohmic resistivity R_Ω is small, i.e., the product $JR_\Omega/b \ll 1$ (see¹⁶ for details). Eqs.(15), (16) allow us to get analytical solution to the problem. A more accurate approximation of \tilde{j}^0 and \tilde{c}^0 can be obtained numerically as discussed in¹⁶.

Local cell impedance at the point \tilde{z} is given by

$$\tilde{Z}_{loc}(\tilde{z}) = \frac{\tilde{\eta}^1}{\tilde{j}^1} \quad (17)$$

To calculate \tilde{Z}_{loc} , we solve Eq.(13):

$$\tilde{c}^1 = \frac{i\tilde{\eta}^1\tilde{\omega} \left(\left(1 - \frac{1}{\lambda}\right)^{\tilde{z}} \exp\left(-\frac{i\tilde{\omega}\psi^2\tilde{z}}{\lambda\tilde{J}}\right) - 1 \right)}{\phi_\lambda\tilde{J} + i\tilde{\omega}\psi^2} + \frac{\tilde{\eta}^1(1 - k_v)\phi_\lambda\tilde{J}}{i\tilde{\omega}\psi^2} \left(1 - \frac{1}{\lambda}\right)^{\tilde{z}} \left(\exp\left(-\frac{i\tilde{\omega}\psi^2\tilde{z}}{\lambda\tilde{J}}\right) - 1 \right) \quad (18)$$

where the parameter ϕ_λ is

$$\phi_\lambda = -\lambda \ln\left(1 - \frac{1}{\lambda}\right), \quad (19)$$

and equation for the static cell polarization curve

$$\phi_\lambda\tilde{J} = e^{\tilde{\eta}^0} \quad (20)$$

was used to eliminate $e^{\tilde{\eta}^0}$ in Eq.(18). Eq.(20) is obtained upon substitution of Eqs.(15), (16) into the static version of charge conservation equation (6).

Substituting Eq.(18) into Eq.(14) and dividing the resulting equation by \tilde{j}^1 , we get an algebraic equation for \tilde{Z}_{loc} . Solving this equation, we come to

$$\tilde{Z}_{loc} = \frac{1}{\phi_\lambda\tilde{J}} \left\{ i \left(\frac{\tilde{\omega}}{\phi_\lambda\tilde{J} + i\tilde{\omega}\psi^2} - \frac{\phi_\lambda\tilde{J}(1 - k_v)}{\tilde{\omega}\psi^2} \right) \times \left(1 - \frac{1}{\lambda}\right)^{\tilde{z}} \exp\left(-\frac{i\tilde{\omega}\psi^2\tilde{z}}{\lambda\tilde{J}}\right) - \frac{i\tilde{\omega}}{\phi_\lambda\tilde{J} + i\tilde{\omega}\psi^2} + \left(1 - \frac{1}{\lambda}\right)^{\tilde{z}} \left(1 + \frac{i\phi_\lambda\tilde{J}(1 - k_v)}{\tilde{\omega}\psi^2}\right) + \frac{i\tilde{\omega}}{\phi_\lambda\tilde{J}} \right\}^{-1} \quad (21)$$

The total cell impedance \tilde{Z}_{cell} is given by

$$\tilde{Z}_{cell} = \left(\int_0^1 \frac{d\tilde{z}}{\tilde{Z}_{loc}} \right)^{-1} \quad (22)$$

Calculation of integral gives

$$\tilde{Z}_{cell} = \left(\left(i\phi_\lambda\tilde{J} - 2\tilde{\omega}\psi^2 \right) \phi_\lambda\tilde{J} - i\tilde{\omega}^2\psi^4 \right) \frac{\tilde{\omega}\psi^2}{D_{cell}} \quad (23)$$

where

$$D_{cell} = (\lambda - 1) \left(1 - \exp\left(-\frac{i\tilde{\omega}\psi^2}{\lambda\tilde{J}}\right) \right) (1 - k_v)\phi_\lambda^3\tilde{J}^4 - \left((1 - k_v) \left(\exp\left(-\frac{i\tilde{\omega}\psi^2}{\lambda\tilde{J}}\right) (\lambda - 1) - \lambda \right) - 2k_v + 1 \right) \times i\tilde{\omega}\psi^2\phi_\lambda^2\tilde{J}^3 - \left((1 + k_v)\psi^2 - \exp\left(-\frac{i\tilde{\omega}\psi^2}{\lambda\tilde{J}}\right) (\lambda - 1) + \lambda \right) \times \tilde{\omega}^2\psi^2\phi_\lambda\tilde{J}^2 - i(\psi^2 + \phi_\lambda)\tilde{\omega}^3\psi^4\tilde{J} + \tilde{\omega}^4\psi^6 \quad (24)$$

III. RESULTS AND DISCUSSION

It is advisable to consider first the limit of $\omega \rightarrow 0$. Expansion of Eq.(23) in Taylor series over $\tilde{\omega} \rightarrow 0$ gives at leading order the differential cell resistivity \tilde{R}_{cell} , which in dimension form is

$$R_{cell} = \frac{b}{J \left(k_v - (\lambda - 1) \ln(1 - 1/\lambda) (1 - k_v) \right)} \quad (25)$$

With $k_v = 0$ (no velocity modulation), Eq.(25) reduces to¹⁵

$$R_{cell}^{k_v=0} = -\frac{b}{J \left((\lambda - 1) \ln(1 - 1/\lambda) \right)} \quad (26)$$

The factor

$$\phi_2 = (\lambda - 1) \ln\left(1 - \frac{1}{\lambda}\right) < 1 \quad (27)$$

in denominator of Eq.26 describes the resistivity growth due to finite air flow stoichiometry λ ; the less is ϕ_2 , the larger is the transport resistivity (Figure 2).

However, with $k_v = 1$ the dependence on λ in Eq.(25) vanishes and we get

$$R_{cell}^{k_v=1} = \frac{b}{J} \quad (28)$$

which is a pure charge-transfer cell resistivity¹⁷. Thus, velocity perturbation with the dimensionless amplitude equal to the amplitude of potential perturbation completely compensates for the losses due to oxygen transport in the cathode channel. The equality of \tilde{v}^1 and $\tilde{\eta}^1$ perturbation amplitudes means that the following relation between the dimension amplitudes must hold:

$$\frac{v^1}{v_*} = \frac{\eta^1}{b} \quad (29)$$

Typical ORR Tafel slope in Pt/C electrodes is about 30 mV.

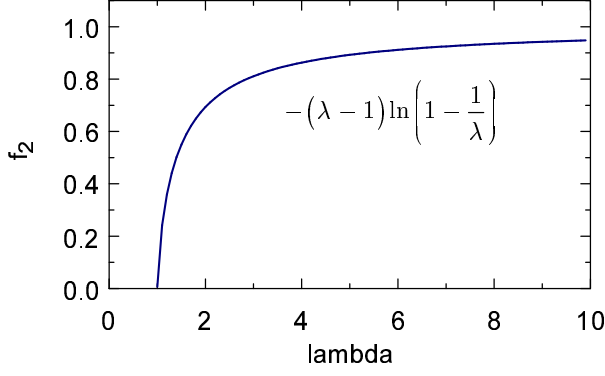


FIG. 2. Function $\phi_2 = -(\lambda - 1) \ln(1 - 1/\lambda)$ appearing in denominator of Eqs.(25),(26).

| | |
|---|-----------|
| Catalyst layer thickness l_t , cm | 10^{-3} |
| Exchange current density i_* , A cm $^{-3}$ | 10^{-3} |
| ORR Tafel slope b , V | 0.03 |
| Double layer capacitance, C_{dl} , F cm $^{-3}$ | 20 |
| Channel depth h , cm | 0.1 |
| Cell temperature T , K | 273 + 80 |
| Mean cell current density J , A cm $^{-2}$ | 0.1 |
| Air flow stoichiometry λ | 2 |

TABLE I. Cell geometrical and operating parameters used in the calculations. The characteristic values of b and C_{dl} are taken from impedance measurements¹⁸; the value of i_* is assumed. The Tafel slope is given per exponential basis.

Thus, with the potential oscillation amplitude on the order of 3 mV, the flow velocity oscillation with the amplitude of 10% of the time-average velocity provides complete compensation of oxygen transport losses in the channel.

With the growth of λ , the effect of velocity modulation progressively lowers. Indeed, setting in Eq.(28) $\phi_2 \simeq 1$, we see that the dependence on k_v vanishes. From Figure 2 it is clear that the effect of velocity modulation is most pronounced at $\lambda \lesssim 2$, which agrees with the experimental results of Kim et al.¹³.

The effect of k_v on the dimension Nyquist spectra of Eq.(22) is shown in Figure 3. With $k_v = 0$, the spectrum has the form of two arcs, with the left arc due to faradaic impedance, and the right arc due to oxygen transport in channel¹. When k_v varies from 0 to 1, the “channel” arc gets smaller, and at $k_v = 1$ this arc almost completely vanishes (Figure 3). The curve $k_v = 1$ illustrates compensation of the “channel” losses by the applied flow velocity oscillations.

To understand the role of velocity oscillations, consider Eq.(14). With $\tilde{c}^1 = 0$ (no perturbation of the oxygen concentration in channel), this equation simplifies to

$$\tilde{j}^1 = \left(e^{\tilde{\eta}^0} \tilde{c}^0 + i\tilde{\omega} \right) \tilde{\eta}^1 \quad (30)$$

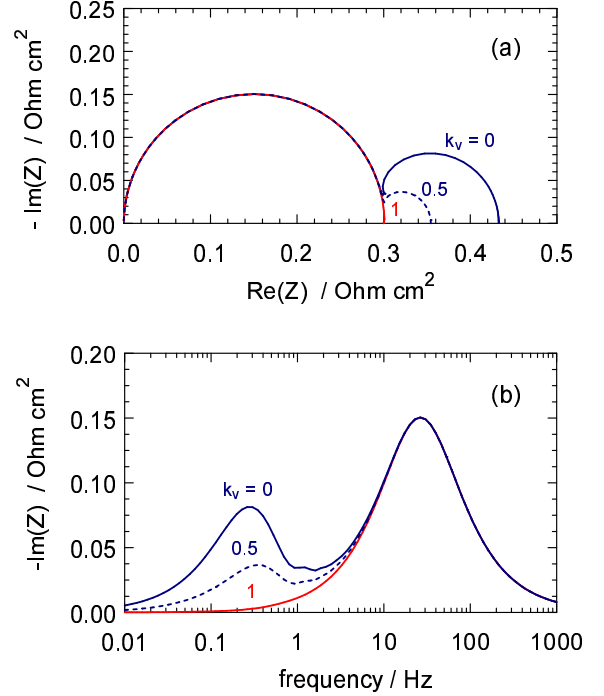


FIG. 3. (a) Nyquist spectra of the total cell impedance, Eq.(23) for the indicated values of the flow velocity amplitude parameter k_v , Eq.(12). Zero k_v corresponds to static flow velocity. (b) The frequency dependence of imaginary part of impedance in (a).

and hence the local cell impedance $\tilde{Z}_{loc} = \tilde{\eta}^1 / \tilde{j}^1$ reduces to impedance of a parallel RC -circuit:

$$\tilde{Z}_{loc}^{\tilde{c}^1=0} = \frac{1}{e^{\tilde{\eta}^0} \tilde{c}^0 + i\tilde{\omega}} = \frac{1}{\tilde{j}^0 + i\tilde{\omega}} \quad (31)$$

Using here \tilde{j}^0 from Eq.(15), and calculating the total cell impedance according to Eq.(22), we get

$$\tilde{Z}_{cell}^{\tilde{c}^1=0} = \frac{1}{\tilde{J} + i\tilde{\omega}} \quad (32)$$

which is pure charge-transfer impedance. Thus, the oxygen transport losses are represented by the term with \tilde{c}^1 in Eq.(14). The trick is that with $k_v = 1$ this term is strongly damped.

Figure 4 shows the real and imaginary part of the normalized oxygen “concentration admittance”

$$Y = \frac{\tilde{c}^1}{\tilde{\eta}^1} \quad (33)$$

obtained from Eq.(18) with $k_v = 0$ and $k_v = 1$. As can be seen, at $k_v = 1$ the amplitude of \tilde{c}^1 oscillations is strongly damped, leading to much lower transport loss.

Note that with $k_v = 1$, Y is still non-zero at $\tilde{\omega} > 0$ (Figure 4), meaning that complete compensation of the channel impedance occurs in the limit of $\tilde{\omega} \rightarrow 0$ only, while at a finite $\tilde{\omega}$, the cell impedance slightly differs from the faradaic impedance, Eq.(32).

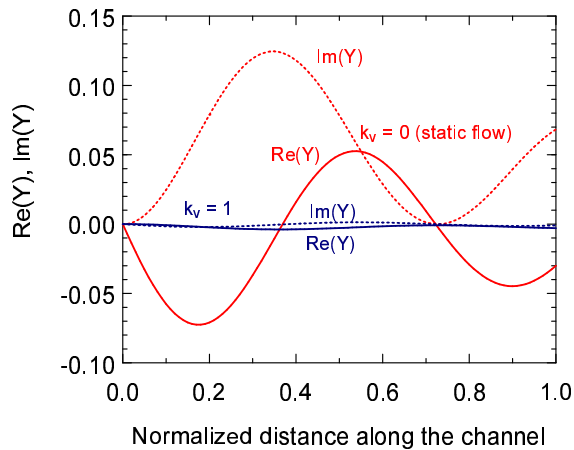


FIG. 4. Normalized oxygen concentration perturbation amplitude $Y = \bar{c}^1/\bar{\eta}^1$, Eqs.(33), (18), along the cathode channel for the two values of the flow velocity amplitude parameter k_v , Eq.(12). The frequency of potential and velocity oscillations $f = 1$ Hz.

From this analysis it follows that the whole effect of oxygen transport loss in channel is purely dynamic in nature. In the true steady state, finite oxygen stoichiometry λ only shifts the polarization curve as a whole along the potential axis, not changing the slope of the curve (cell resistivity). Indeed, from the static polarization curve, Eq.(20), it follows that the true static differential cell resistivity $R_{cell}^0 = \partial\bar{\eta}^0/\partial\bar{J} = 1/\bar{J}$, which is a pure faradaic resistivity independent of λ . This result also follows from Eq.(32) However, small perturbations of flow parameters immediately lead to small oscillations of oxygen concentration in channel. These oscillations, in turn, induce small oscillations of the cell potential, and the system enters the dynamic mode with the quasi-static resistivity given by Eq.(26). Harmonic modulation of the flow velocity with $0 < k_v \leq 1$ allows one to lower this resistivity, as Eq.(25) shows.

In reality, fuel cell never works in a true steady state; due to small variation of operating conditions and aging of cell components, even in stationary experiments and applications the cell potential slowly varies with time. This variation corresponds to a small but nonzero $\tilde{\omega} > 0$, making the “channel” resistivity quite significant. In automotive applications, fuel cells operate in intrinsically transient regimes and the cell voltage strongly varies with time.

In this work, AC perturbation $\bar{\eta}^1$ of the cell potential and the velocity oscillation amplitude k_v are assumed to be independent parameters. However, in real applications, the amplitude of flow velocity oscillations could be regulated by flow controller, while the respective potential perturbation would be a dependent, uncontrolled parameter. The relation between oscillation amplitudes of velocity and cell potential in this case could be controlled experimentally. Another option would be excitation of flow velocity oscillations by pressure wave applied to the inlet flow. However, development of impedance model which would describe this situation is a much more challenging task. The experiments^{14,19} and

the simple model above suggest that the problem deserves further studies.

IV. CONCLUSIONS

The model of PEM fuel cell impedance is developed taking into account air flow velocity oscillations applied in-phase with the AC potential perturbation. The model is based on oxygen mass transport equation in the cathode channel coupled to the proton current conservation equation in the cathode catalyst layer. The model aims at description of low-frequency phenomena in the cell and it ignores proton and oxygen transport in the porous layers, assuming that this transport is fast.

The model shows that velocity oscillations reduce the resistivity R_h of oxygen transport in the cathode channel. If the relative amplitudes of velocity and potential oscillations are equal, the resistivity R_h vanishes. These results explain experimental findings of Kim et al.¹³ and Hwang et al.¹⁴ who demonstrated dramatic improvement of PEM fuel cell performance under oscillating air flow velocity.

- ¹I. A. Schneider, S. A. Freunberger, D. Kramer, A. Wokaun and G. G. Scherer, *Oscillations in Gas Channels. Part I. The Forgotten Player in Impedance Spectroscopy in PEFCs*, J. Electrochem. Soc. **154** (2007), pp. B383–B388
- ²I. A. Schneider, D. Kramer, A. Wokaun and G. G. Scherer, *Oscillations in Gas Channels. II. Unraveling the Characteristics of the Low-Frequency Loop in Air-Fed PEFC Impedance Spectra*, J. Electrochem. Soc. **154** (2007), pp. B770–B782
- ³T. V. Reshetenko, G. Bender, K. Bethune and R. Rocheleau, *Systematic Study of Back Pressure and Anode Stoichiometry Effects on Spatial PEMFC Performance Distribution*, Electrochim. Acta **56** (2011), pp. 8700–8710
- ⁴T. V. Reshetenko, J. St-Pierre, K. Artyushkova, R. Rocheleau, P. Atanassov, G. Bender and M. Ulsh, *Multianalytical Study of the PTFE Content Local Variation of the PEMFC Gas Diffusion Layer*, J. Electrochem. Soc. **160** (2013), pp. F1305–F1315
- ⁵N. Zamel, A. Bhattarai and D. Gerteisen, *Measurement of Spatially Resolved Impedance Spectroscopy with Local Perturbation*, Fuel Cells **13** (2013), pp. 910–916
- ⁶A. A. Kulikovskiy, *A Model for Local Impedance of the Cathode Side of PEM Fuel Cell With Segmented Electrodes*, J. Electrochem. Soc. **159** (2012), pp. F294–F300
- ⁷C. Bao and W. G. Bessler, *Two-Dimensional Modeling of a Polymer Electrolyte Membrane Fuel Cell with Long Flow Channel. Part II. Physics-Based Electrochemical Impedance Analysis*, J. Power Sources **278** (2015), pp. 675–682
- ⁸A. Kulikovskiy and O. Shamardina, *A Model for PEM Fuel Cell Impedance: Oxygen Flow in the Channel Triggers Spatial and Frequency Oscillations of the Local Impedance*, J. Electrochem. Soc. **162** (2015), pp. F1068–F1077
- ⁹S. Chevalier, C. Josset, A. Bazylak and B. Auvity, *Measurements of Air Velocities in Polymer Electrolyte Membrane Fuel Cell Channels Using Electrochemical Impedance Spectroscopy*, J. Electrochem. Soc. **163** (2016), pp. F816–F823
- ¹⁰A. Kulikovskiy, *A Fast Low-Current Model for Impedance of a PEM Fuel Cell Cathode at Low Air Stoichiometry*, J. Electrochem. Soc. **164** (2017) (9), pp. F911–F915
- ¹¹S. Chevalier, C. Josset and B. Auvity, *Analytical Solution for the Low Frequency Polymer Electrolyte Membrane Fuel Cell Impedance*, J. Power Sources **407** (2018), pp. 123–131
- ¹²T. Reshetenko and A. Kulikovskiy, *A Model for Extraction of Spatially Resolved Data from Impedance Spectrum of a PEM Fuel Cell*, J. Electrochem. Soc. **165** (2018), pp. F291–F296
- ¹³Y. H. Kim, H. S. Han, S. Y. Kim and G. H. Rhee, *Influence of Cathode Flow Pulsation on Performance of Proton-Exchange Membrane Fuel Cell*, J. Power Sources **185** (2008), pp. 112–117

- ¹⁴Y.-S. Hwang, D.-Y. Lee, J. W. Choi, S.-Y. Kim, S. H. Cho, P. Joonho, M. S. Kim, J. H. Jang, S. H. Kim and S.-W. Cha, *Enhanced Diffusion in Polymer Electrolyte Membrane Fuel Cells Using Oscillating Flow*, Int. J. Hydrogen Energy **35** (2010), pp. 3676–3683
- ¹⁵A. Kulikovskiy, *Analytical Impedance of Oxygen Transport in a PEM Fuel Cell Channel*, J. Electrochem. Soc. **166** (2019), pp. F306–F311
- ¹⁶T. Reshetenko and A. Kulikovskiy, *On the Distribution of Local Current Density Along the PEM Fuel Cell Cathode Channel*, Electrochem. Comm. **101** (2019), pp. 35–38
- ¹⁷A. A. Kulikovskiy, *One-Dimensional Impedance of the Cathode Side of a PEM Fuel Cell: Exact Analytical Solution*, J. Electrochem. Soc. **162** (2015), pp. F217–F222
- ¹⁸T. Reshetenko and A. Kulikovskiy, *Comparison of Two Physical Models for Fitting PEM Fuel Cell Impedance Spectra Measured at a Low Air Flow Stoichiometry*, J. Electrochem. Soc. **163** (2016), pp. F238–F246
- ¹⁹K.-H. Kim, H.-J. Kim, K.-Y. Lee, J. H. Jang, S.-Y. Lee, E. Cho, I.-H. Oh and T.-H. Lim, *Effect of Nafions Gradient in Dual Catalyst Layer on Proton Exchange Membrane Fuel Cell Performance*, Int. J. Hydrogen Energy **33** (2008), pp. 2783 – 2789

Nomenclature

| | |
|-----------|---|
| \sim | Marks dimensionless variables |
| b | ORR Tafel slope, V |
| C_{dl} | Double layer volumetric capacitance, F cm ⁻³ |
| c | Oxygen molar concentration, mol cm ⁻³ |
| c_{ref} | Reference oxygen concentration (at the channel inlet), mol cm ⁻³ |
| F | Faraday constant, C mol ⁻¹ |
| f | Regular frequency, Hz |
| J | Mean cell current density, A cm ⁻² |
| j | Local cell current density, A cm ⁻² |
| h | Channel depth, cm |
| i | Imaginary unit |
| i_* | Volumetric exchange current density, A cm ⁻³ |
| L | Channel length, cm |
| l_t | Catalyst layer thickness, cm |
| t | Time, s |
| v | Flow velocity in the cathode channel, cm s ⁻¹ |
| x | Coordinate through the cell, cm |
| Z | Impedance, Ω cm ² |
| z | Coordinate along the air channel, cm |

Subscripts:

| | |
|-------|--------------------------------------|
| h | Air channel |
| loc | Local impedance |
| * | Characteristic or time-average value |

Superscripts:

| | |
|---|------------------------------|
| 0 | Steady-state value |
| 1 | Small-amplitude perturbation |

Greek:

| | |
|----------------|--|
| λ | Air flow stoichiometry |
| ϕ_λ | Dimensionless parameter, Eq.(19) |
| ψ | Dimensionless parameter, Eq.(7) |
| ω | Angular frequency ($\omega = 2\pi f$), s ⁻¹ |